

Lithosphere

Extension-driven right-lateral shear in the Centennial shear zone adjacent to the eastern Snake River Plain, Idaho

S.J. Payne, R. McCaffrey and S.A. Kattenhorn

Lithosphere published online 3 June 2013;
doi: 10.1130/L200.1

Email alerting services

click www.gsapubs.org/cgi/alerts to receive free e-mail alerts when new articles cite this article

Subscribe

click www.gsapubs.org/subscriptions/ to subscribe to Lithosphere

Permission request

click <http://www.geosociety.org/pubs/copyrt.htm#gsa> to contact GSA

Copyright not claimed on content prepared wholly by U.S. government employees within scope of their employment. Individual scientists are hereby granted permission, without fees or further requests to GSA, to use a single figure, a single table, and/or a brief paragraph of text in subsequent works and to make unlimited copies of items in GSA's journals for noncommercial use in classrooms to further education and science. This file may not be posted to any Web site, but authors may post the abstracts only of their articles on their own or their organization's Web site providing the posting includes a reference to the article's full citation. GSA provides this and other forums for the presentation of diverse opinions and positions by scientists worldwide, regardless of their race, citizenship, gender, religion, or political viewpoint. Opinions presented in this publication do not reflect official positions of the Society.

Notes

Advance online articles have been peer reviewed and accepted for publication but have not yet appeared in the paper journal (edited, typeset versions may be posted when available prior to final publication). Advance online articles are citable and establish publication priority; they are indexed by GeoRef from initial publication. Citations to Advance online articles must include the digital object identifier (DOIs) and date of initial publication.

Extension-driven right-lateral shear in the Centennial shear zone adjacent to the eastern Snake River Plain, Idaho

S.J. Payne¹, R. McCaffrey², and S.A. Kattenhorn³

¹IDAHO NATIONAL LABORATORY, P.O. BOX 1625, MS 2203, IDAHO FALLS, IDAHO 83415, USA

²DEPARTMENT OF GEOLOGY, PORTLAND STATE UNIVERSITY, P.O. BOX 751, PORTLAND, OREGON 97207, USA

³DEPARTMENT OF GEOLOGICAL SCIENCES, UNIVERSITY OF IDAHO, P.O. BOX 443022, MOSCOW, IDAHO 83844, USA

ABSTRACT

We evaluate global positioning system (GPS) surface velocities and gravitational potential energy (GPE) variations to assess the causes of right-lateral shear in the Centennial shear zone, a NE-trending accommodation zone between the extensional Centennial tectonic belt (Montana-Idaho) and volcanic terrain of the eastern Snake River Plain (Idaho). We test the hypothesized “bookshelf” faulting model and find that the normal faults in the Centennial tectonic belt do not accommodate distributed dextral shear. Instead, GPS data reveal that rapid extension in the Centennial tectonic belt adjacent to the much more slowly deforming region of the Snake River Plain drives right-lateral shear between them at rates of 0.3–1.5 mm yr⁻¹. GPE variations support gravitational collapse at a higher rate in the Centennial tectonic belt due to higher topography than in eastern Snake River Plain, which has lower GPE variations due to its low-relief, flat topography and a denser crustal composition. Surface velocity gradients observed in GPS data across the 40–45-km-wide Centennial shear zone reveal distributed deformation due to strike-slip faulting, distributed simple shear, regional-scale rotation, or some combination thereof. In the Centennial shear zone, the fastest lateral shearing is closest to the Yellowstone Plateau, where fault plane solutions with components of right-lateral strike slip are documented within a NE-trending zone of seismicity. Here, two Basin and Range normal faults have Holocene and late Pleistocene slip along their segments that suggest they each may have linked under right-lateral shear. We also propose that right-lateral strike-slip motion may be accommodated on existing NE-trending faults.

LITHOSPHERE

GSA Data Repository Item 2013226

doi: 10.1130/L200.1

INTRODUCTION

Previous studies (Chadwick et al., 2007; Holmes et al., 2008; Payne et al., 2008, 2012) have documented the different strain rates between the volcanic province of the eastern Snake River Plain and the Basin and Range region to the northwest within the Centennial tectonic belt (Stickney and Bartholomew, 1987) in Idaho and Montana. Payne et al. (2012) evaluated 405 global positioning system (GPS) velocities in the northern Basin and Range Province to show that the Centennial tectonic belt is extending at a much faster rate ($5.6 \pm 0.7 \times 10^{-9}$ yr⁻¹) than the Snake River Plain ($-0.1 \pm 0.4 \times 10^{-9}$ yr⁻¹, which is not discernible from zero). Deformation in the intervening Centennial shear zone was proposed by Payne et al. (2008, 2012) to be a consequence of these different horizontal strain rates. This assertion is controversial since the boundary between the eastern Snake River Plain and Centennial tectonic belt, along which a shear zone is implied by GPS, lacks mapped strike-slip faults (e.g., Kuntz et al., 1994; Rodgers et al., 2002; Holmes et al., 2008). The absence of discernible strike-slip offset in the geology at the termination of the normal faults has led to the hypothesis that extension by normal faulting in the Centennial tectonic belt and extension by dike intrusion in the eastern Snake River Plain occur at similar rates (Rodgers et al., 1990, 2002; Parsons et al., 1998), an interpretation seemingly at odds with the new GPS results.

Using geological, geophysical, and seismological data, and the 1994–2010 GPS velocity field presented in Payne et al. (2012), we investigated the cause and effect of right-lateral shear (Fig. 1A). Specifically, we assessed whether shear is a consequence of the different strain rates between the Cen-

ennial tectonic belt and eastern Snake River Plain or, alternatively, if right-lateral shear at its edges drives normal faulting (i.e., “bookshelf” faulting) over the entire Centennial tectonic belt. Different strain rates could derive from differences in gravitational potential energy (GPE), i.e., gravitational collapse at a higher rate in the higher topographic relief of the Centennial tectonic belt versus a lower rate within the relatively flat region of the eastern Snake River Plain. In this case, shear would result from extension at a higher rate in the Centennial tectonic belt region than in the adjacent slowly deforming eastern Snake River Plain (e.g., Payne et al., 2012). In the case of the bookshelf faulting hypothesis, normal faulting is driven by edge shear stress. That is, oblique-normal fault slip and clockwise rotation of the fault-bounded ranges within the Centennial tectonic belt are driven by, and accommodate, distributed right-lateral shear over the entire zone (e.g., McKenzie and Jackson, 1986). If corroborated by the GPS data, bookshelf faulting would be consistent with the lack of geologic evidence for strike-slip boundary faults.

To explore these two hypotheses, we first used block models constrained by GPS and earthquake data to find a range of acceptable tectonic models. We build upon the approach of Payne et al. (2012), who, through a series of rigorous tests, determined a preferred tectonic block model that fits the GPS and earthquake data in the northern Basin and Range Province. We modified the preferred block model to evaluate the bookshelf-style faulting model proposed by McKenzie and Jackson (1986) in the Centennial tectonic belt. Next, we calculated the GPE of the Centennial tectonic belt and eastern Snake River Plain using recently derived density models of DeNosaquo et al. (2009) to test whether GPE variations could drive extension. To reveal the effects of crustal density perturbations and

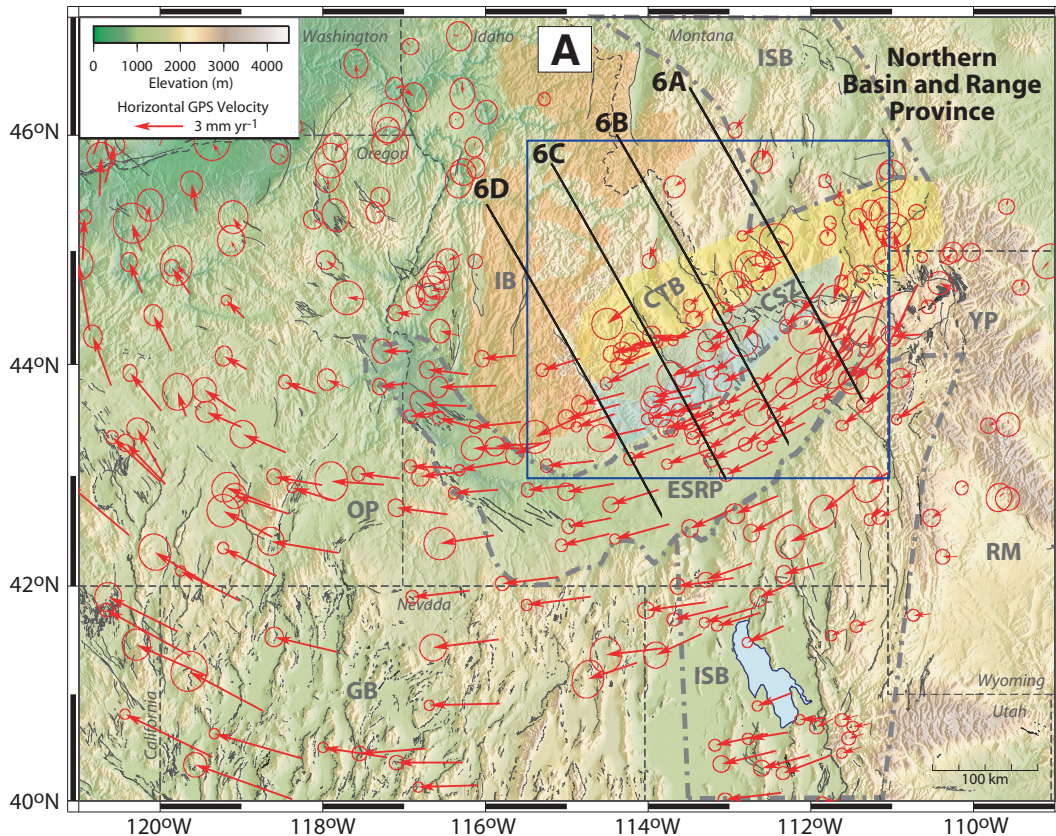
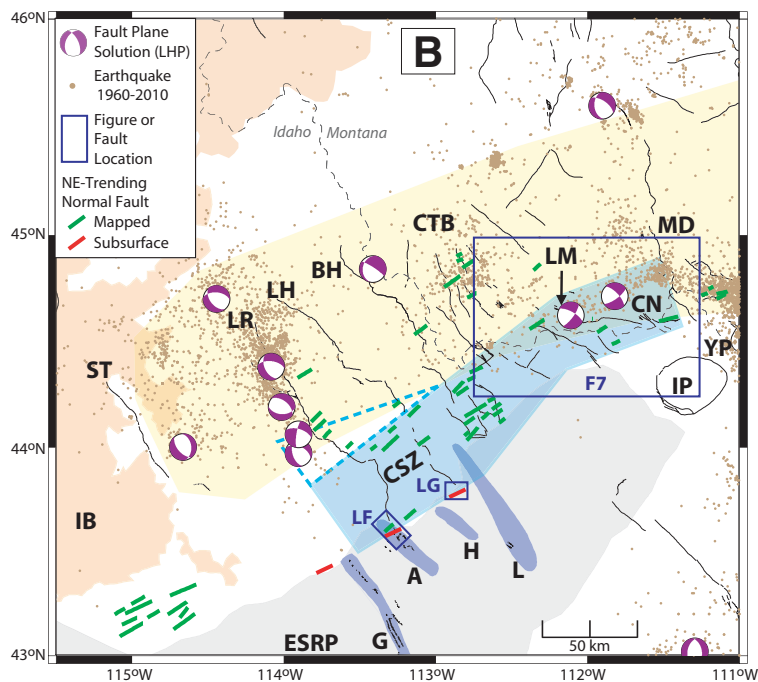


Figure 1. (A) Shaded relief map showing 1994–2010 observed global positioning system (GPS) horizontal velocities (red vectors) and their 70% confidence ellipses in the stable North American reference frame (modified from Payne et al., 2012). Profile lines refer to Figure 6, and box indicates map boundaries of study region (Figs. 1B, 2, 4, and 5A). The Centennial shear zone (blue region) is shown as defined by Payne et al. (2012). (B) Map showing interpretation of the Centennial



shear zone (blue shaded regions, dashed lines where inferred) from this study. Geologic features include mapped NE-trending faults (green lines) modified from Zentner (1989), and subsurface faults (red lines) identified from geophysical data (Sparlin et al., 1982; Pankratz and Ackerman, 1982; Young and Lucas, 1988). Blue boxes labeled “LF” and “LG” are locations discussed in the text, and “F7” indicates the box for Figure 7. Volcanic rift zones (dark blue shading) are labeled for Arco (A), Great Rift (G), Howe–East Butte (H), and Lava Ridge–Hell’s Half Acre (L). Lower-hemisphere fault plane (LHP) solutions are listed in Table DR2 in the GSA Data Repository (see text footnote 1). Earthquake epicenters (brown dots) were compiled for magnitudes greater than 2.0 from 1960 to 2011 (Advanced National Seismic System, 2011). Dashed-dotted lines in A and shaded regions in both A and B show tectonic provinces. Abbreviations include: CTB—Centennial tectonic belt (Stickney and Bartholomew, 1987); CSZ—Centennial shear zone; ESRP—eastern Snake River Plain; GB—Great Basin; IB—Idaho Batholith (Bond et al., 1978; Stoesser et al., 2005); IP—Island Park; ISB—Intermountain Seismic Belt (Smith and Arabasz, 1991); OP—Owyhee–Oregon Plateau; RM—Rocky Mountains; SRP—Snake River Plain; and YP—Yellowstone Plateau. Thin black lines show Quaternary faults (U.S. Geological Survey, 2007). Holocene normal faults are labeled for the Beaverhead (BH), Centennial (CN), Lemhi (LH), Lima Reservoir (LM), Lost River (LR), Madison (MD), and Sawtooth (ST) faults. This figure and others were generated using the Generic Mapping Tool (Wessel and Smith, 1998).

differences in topography on GPE variations, we evaluated the GPE of the two regions using density models that either included or excluded a mid-crustal sill and lower-crustal partial melt and underplated layers within the eastern Snake River Plain. Finally, we integrated the GPS and GPE results with geological, geophysical, and seismological data to assess the role of shear and propose boundaries and mechanisms of distributed shear within the Centennial shear zone. We present supporting observations from contemporary seismicity and offer possible examples of locations where shear may be accommodated along existing faults.

GEOLOGIC SETTING

We present a short discussion of geologic features and earthquake activity that have relevance to the kinematic interpretations of the GPS and discuss crustal compositions that affect density models used to estimate GPE variations. The study region includes the eastern Snake River Plain, Centennial tectonic belt, and the proposed Centennial shear zone located in the northern Basin and Range Province (Fig. 1). The eastern Snake River Plain encompasses Late Tertiary silicic volcanic centers that represent the NE-trending track of the Yellowstone hotspot, which is currently located beneath the Yellowstone Plateau (Pierce and Morgan, 1992, 2009; Morgan and McIntosh, 2005). Mafic intrusions into the midcrust caused partial melting of crustal rocks, producing large-volume silicic eruptions from ca. 10 Ma to 4 Ma, which were later followed by basalt dike intrusions that have continued into the Holocene and are concentrated in NW-trending volcanic rift zones (Fig. 1B) (Kuntz et al., 1986, 1992). The large influx of mafic magma and eruptions have altered the Snake River Plain topography and crust, leaving behind a relatively flat region underlain by a 10–16-km-thick mafic sill at mid- to lower-crustal depths (10–30 km; e.g., Sparlin et al., 1982; Peng and Humphreys, 1998; Stachnik et al., 2008; Yuan et al., 2010). DeNosaquo et al. (2009) employed gravity, seismic, thermal, rheological, and petrological data to model the density structure of the crust, which includes a zone of partial melt and thickened (or underplated) lower crust below the midcrustal sill. Conversely, seismic refraction indicates that the crust beneath the Centennial tectonic belt is unaltered by hotspot volcanism. Upper- and lower-crustal compression-wave velocities (Sheriff and Stickney, 1984; Stickney, 1997) are consistent with those determined by DeNosaquo et al. (2009) for the Basin and Range regions north and south of the eastern Snake River Plain.

The Basin and Range region northwest of the eastern Snake River Plain is characterized by prominent Quaternary normal faults, short NE-trending normal faults, and higher seismic activity. It includes two zones of normal faulting: (1) the Centennial tectonic belt, a zone of Holocene faulting with mountain ranges >0.7 km high and high seismicity (Stickney and Bartholomew, 1987); and (2) Faulting Belt III of Pierce and Morgan (1992; 2009), a zone of major late Pleistocene (<130 ka) faulting with mountain ranges <0.5 km high and low seismicity. For simplicity, we refer to the entire region as the Centennial tectonic belt and note that the proposed Centennial shear zone is located along the southeast boundary of the Centennial tectonic belt adjacent to the eastern Snake River Plain (Fig. 1).

The Centennial tectonic belt includes three ~150-km-long, NW-trending normal faults (Lost River, Lemhi, and Beaverhead; Fig. 1B) that have southwest dips and over 2 km of relief along their ranges. Extension across these three faults may have begun ca. 16 Ma based on interpretations of typical half-graben basin fill and the age of intercalated volcanic ash at the southern end of the Lemhi fault (Rodgers et al., 2002). Recent faulting is evidenced by the 1983 moment magnitude (*M*) 6.9 Borah Peak, Idaho, earthquake, which ruptured the central segment of the Lost River fault with oblique normal slip that included a 17% sinistral component (Crone et al., 1987). At the southern ends of the three normal faults and within the

proposed Centennial shear zone, bedrock structural features inferred from gravity and seismic-reflection data suggest that significant fault offsets do not extend into the eastern Snake River Plain (Mabey, 1978; Jackson et al., 2006). However, short and generally left-stepping, en echelon, NW-trending normal faults and monoclinical flexures expressed in 400–730 ka basalt flows within the eastern Snake River Plain may be interpreted as slip on the Lost River fault (Kuntz et al., 1994, 2002). Alternatively, Smith et al. (1996) associated the short normal faults, monoclines, fissures, and nearby volcanic vents collectively as deformation produced from intruding dikes in the Arco volcanic rift zone (blue box labeled “LF” in Fig. 1B). Farther northeast and in southwest Montana, there are two notable normal faults within the proposed Centennial shear zone: the E-trending, N-dipping Centennial and NW-trending, SW-dipping Lima Reservoir faults (Fig. 1B). Scarp analyses of the Centennial fault indicate that it formed by a series of NW-trending, left-stepping, en echelon faults compatible with distributed dextral shear, which gives the appearance of an overall eastward trend (Petrik, 2008). The eastern end of the Lima Reservoir fault overlaps with the western end of the Centennial fault, forming two oppositely dipping normal faults interpreted to accommodate right-lateral transtension (Majerowicz et al., 2007; Majerowicz, 2008; Anastasio et al., 2010). Mid-Pleistocene to Holocene slip is evident along segments of the Lima Reservoir and Centennial normal faults (Bartholomew et al., 2002; Majerowicz, 2008; Petrik, 2008; Anastasio et al., 2010), and slip along the Centennial fault may have initiated at 2 Ma (Petrik, 2008).

The decrease in peak elevation of mountain ranges within the Centennial tectonic belt toward the eastern Snake River Plain is interpreted to reflect downwarping due to subsidence of the eastern Snake River Plain (e.g., Kirkham, 1931; Suppe et al., 1975; McQuarrie and Rodgers, 1998; Rodgers et al., 2002). McQuarrie and Rodgers (1998) interpreted NE-trending normal faults to represent extension perpendicular to the Snake River Plain due to crustal flexure resulting from subsidence of the Snake River Plain. The majority of these short NE-trending normal faults (green lines in Fig. 1B) are within the proposed Centennial shear zone (e.g., Zentner, 1989; Janecke, 1992; Rodgers et al., 2002). Additionally, geophysical investigations reveal subsurface normal faults (presumably NE-trending) at three locations along the NE-trending physiographic boundary (red lines in Fig. 1B) of the eastern Snake River Plain (Sparlin et al., 1982; Pankratz and Ackerman, 1982; Stanley, 1982; Elbring, 1984; Young and Lucas, 1988).

The Centennial tectonic belt has higher seismic activity than the eastern Snake River Plain (Fig. 1B). In the Centennial tectonic belt, earthquakes along the NW-trending faults have normal fault plane solutions with NW-oriented nodal planes (Richins et al., 1987; Herrmann et al., 2011). Included among the normal fault events are those for the 1983 *M* 6.9 Borah Peak main shock and aftershocks along the Lost River fault. Farther northeast, near the Lima Reservoir and Centennial faults and within the proposed Centennial shear zone, fault plane solutions are mixed, with a variety of oblique normal slip, strike slip, and even oblique reverse slip (Stickney, 1997, 2007). Evaluation of focal depths and N-dipping nodal planes suggest that only eight events (*M* < 4.4) may be associated with slip on the Centennial normal fault (Stickney, 2007). The majority of the fault plane solutions (*M* < 4.6) are strike slip and have right-lateral motion along NE-trending nodal planes. They are located within a NE-trending zone of seismicity that is oblique to the E trend of the Centennial fault (Fig. 1B).

METHODS AND RESULTS

GPS Data

We used the 1994–2010 GPS-derived surface velocity field presented in Payne et al. (2012) that consists of 405 continuous and survey-mode

GPS sites (Fig. 1A), which includes new sites in eastern Oregon, Idaho, western Wyoming, and southwestern Montana. The velocities were determined relative to the stable North American reference frame (SNARF) using the methods discussed in Payne et al. (2012) (also see GSA Data Repository¹). Figure 1A shows that the 1994–2010 velocity field has gradients that could result from components of rotation or strain or both. Changes in magnitudes of the velocities are clearly visible in the Centennial tectonic belt, whereas more uniform velocities are observed in the eastern Snake River Plain. Additionally, gradients due to regional-scale clockwise rotation are evident over much of the northern Basin and Range Province, including the Centennial tectonic belt and eastern Snake River Plain. In the subsequent interpretations, we exclude those horizontal GPS velocities for which both components have one-sigma uncertainties greater than 0.8 mm yr⁻¹.

Kinematic Interpretations of GPS

To interpret the velocity field, we applied the block-model inverse approach in TDEFNODE (McCaffrey, 2009), which allows us to test mechanisms of deformation using either discrete boundaries or continuous deformation. We inverted GPS velocities and earthquake slip vectors to solve simultaneously for the angular velocities of blocks and uniform, horizontal strain rate tensors within selected blocks. The best fit to the data was found by downhill simplex minimization (Press et al., 1989), an optimization algorithm that minimizes the reduced chi-squared (χ_{η}^2) of the misfit to the weighted data. We compared the statistical significance between two models using the χ_{η}^2 and degrees-of-freedom in F-distribution tests. This approach was used by Payne et al. (2012) to determine a preferred block model (ctb9) for the Centennial tectonic belt and Snake River Plain as part of their entire model encompassing the northern Basin and Range Province. Model ctb9 was determined from a series of tests in which boundaries were systematically added to separate blocks representing tectonic provinces until no statistically significant improvement to the data fit was found. The boundaries were selected based on knowledge of geology, seismicity, volcanism, active tectonic faults, and regions with observed differences in surface velocities. For those tests, a maximum confidence level of $\geq 99\%$ indicated one model with added boundaries had a better fit to the data over a second model (Stein and Gordon, 1984). Variations of model ctb9 were also used by Payne et al. (2012) to test for the presence of dike-opening (i.e., extension) in the Snake River Plain and postseismic relaxation following recent earthquakes. In this study, we altered the preferred model ctb9 of Payne et al. (2012) to set up model csz9, which has a block model configuration that then permitted us to test kinematic models of shear.

Model csz9 and the preferred model of Payne et al. (2012) are tests of whether or not shear between the eastern Snake River Plain and Centennial tectonic belt is the result of different strain rates within them. Model csz9 has nine blocks representing eastern Washington (EWAs), eastern Oregon (EOre), Idaho-Wyoming border (IdWy), Great Basin (GrBn), southwest Montana (SwMT), eastern Montana (EMnt), Idaho batholith (IBat), Centennial tectonic belt (CTBt), and the Snake River Plain combined with the Owyhee-Oregon Plateau (SRPn). Model csz9 differs from

Payne et al. (2012); we separate the CTBt block from the SwMT and EMnt blocks and combine the SwMT and EWAs blocks together, creating boundaries along the NW and SE sides of the CTBt block (Fig. 2A). Strain rates were estimated for the Centennial tectonic belt, Snake River Plain–Owyhee-Oregon Plateau, and Great Basin. We found that model csz9 has a $\chi_{\eta}^2 = 1.18$ (Table 1) and estimated strain rates (positive values for extension) of $6.6 \pm 0.9 \times 10^{-9}$ yr⁻¹ for the CTBt block and $-0.1 \pm 1.1 \times 10^{-9}$ yr⁻¹ for the SRPn block; the latter is not distinguishable from zero (Fig. 2A). Model csz9 has a similar fit to the data as the preferred model of Payne et al. (2012) (see block models in GSA Data Repository for details and comparisons [see footnote 1]). Model csz9 also predicts right-lateral strike-slip motions that vary from 0.3 mm yr⁻¹ to 1.5 mm yr⁻¹ along the NE-trending boundary between the CTBt and SRPn blocks near the Lost River and Centennial faults, respectively.

To test for bookshelf faulting, we employed a model mimicking distributed deformation by oblique faulting and rotating blocks presented by McKenzie and Jackson (1986), which they suggested accommodates right-lateral shear between the eastern Snake River Plain and the Centennial tectonic belt. They interpreted changes in direction from E-oriented extension of the Intermountain seismic belt to NE-oriented extension in the Centennial tectonic belt to involve a component of right-lateral strike slip. Their two-dimensional model has a system of small blocks bounded by parallel, equally spaced normal faults that take up deformation within a deforming zone between two bounding plates in relative motion (McKenzie and Jackson, 1983). Only movement normal to the bounding plates can produce a change in surface area, and so line A-B (Fig. 3A) must remain a constant length and parallel to the strike of the zone boundaries. As shown in Figure 3A, a component of strike-slip motion (dextral) across the deforming zone leads to clockwise rotation (semicircular red arrows) of the ranges and to a component of strike-slip motion (red arrow pairs) in the opposite sense (sinistral) on the block-bounding normal faults.

With this model concept in mind, we performed and compared four tests of the bookshelf-faulting model using variations of block model csz9. In our first test (model cz91), we restricted right-lateral strike-slip motion to be low (≤ 0.2 mm yr⁻¹) along the NW and SE sides of the CTBt block (Fig. 2B). Limiting slip rates along the NW and SE sides, to comply with geologic constraints, allows right-lateral shear to be taken up by distributed deformation within the deforming zone of the CTBt block (i.e., oblique normal slip on normal faults within the block). Model cz91 (Fig. 2B) shows that by limiting strike-slip rates along the NW and SE sides of the CTBt block, a larger component of contraction is predicted at an azimuth of 120° with a strain rate of $-6.3 \pm 1.2 \times 10^{-9}$ yr⁻¹ (Fig. 2B), rather than extension as in model csz9. Model cz91 also has a degraded fit to the GPS and earthquake data ($\chi_{\eta}^2 = 1.30$), and we reject it as a viable alternative model at the 90% probability (Table 2) when compared to model csz9 ($\chi_{\eta}^2 = 1.18$).

In the final three tests using different ranges of rotation rates, we assessed whether or not the mountain ranges bounded by three NW-trending normal faults (Lost River, Lemhi, and Beaverhead faults) in the Centennial tectonic belt rotate at sufficiently fast rates to accommodate distributed shear over the entire zone (Fig. 3A). For these three block model configurations, we added block boundaries along the three NW-trending normal faults, which allowed us to constrain the rotations of the four intervening blocks (BoPk—Borah Peak, Lemh—Lemhi, LsRv—Lost River, and WMnt—western Montana; Fig. 2C) to be clockwise and to assess the sense of slip along the faults. The rotation rates in model cz55 match the velocity gradient across the entire Centennial tectonic belt, and, in models cz52 and cz56, two different ranges of rotation rates are based on paleomagnetic data. In model cz55, we allowed the four blocks to rotate between -0.50° and -0.55° m.y.⁻¹ (clockwise rotation, as seen from

¹GSA Data Repository item 2013226, containing data and calculations of the strain rate shown in Figure 3B, calculation of rotation rate from velocity, earthquake fault plane solutions and their references, descriptions and results of each block model used in the inversions, a brief summary for calculating the velocities using the Snake River Plain frame of reference, results of gravitational potential energy calculations, and references cited in the data repository, is available online at www.geosociety.org/pubs/ft2013.htm, or on request from editing@geosociety.org or Documents Secretary, GSA, P.O. Box 9140, Boulder, CO 80301, USA.

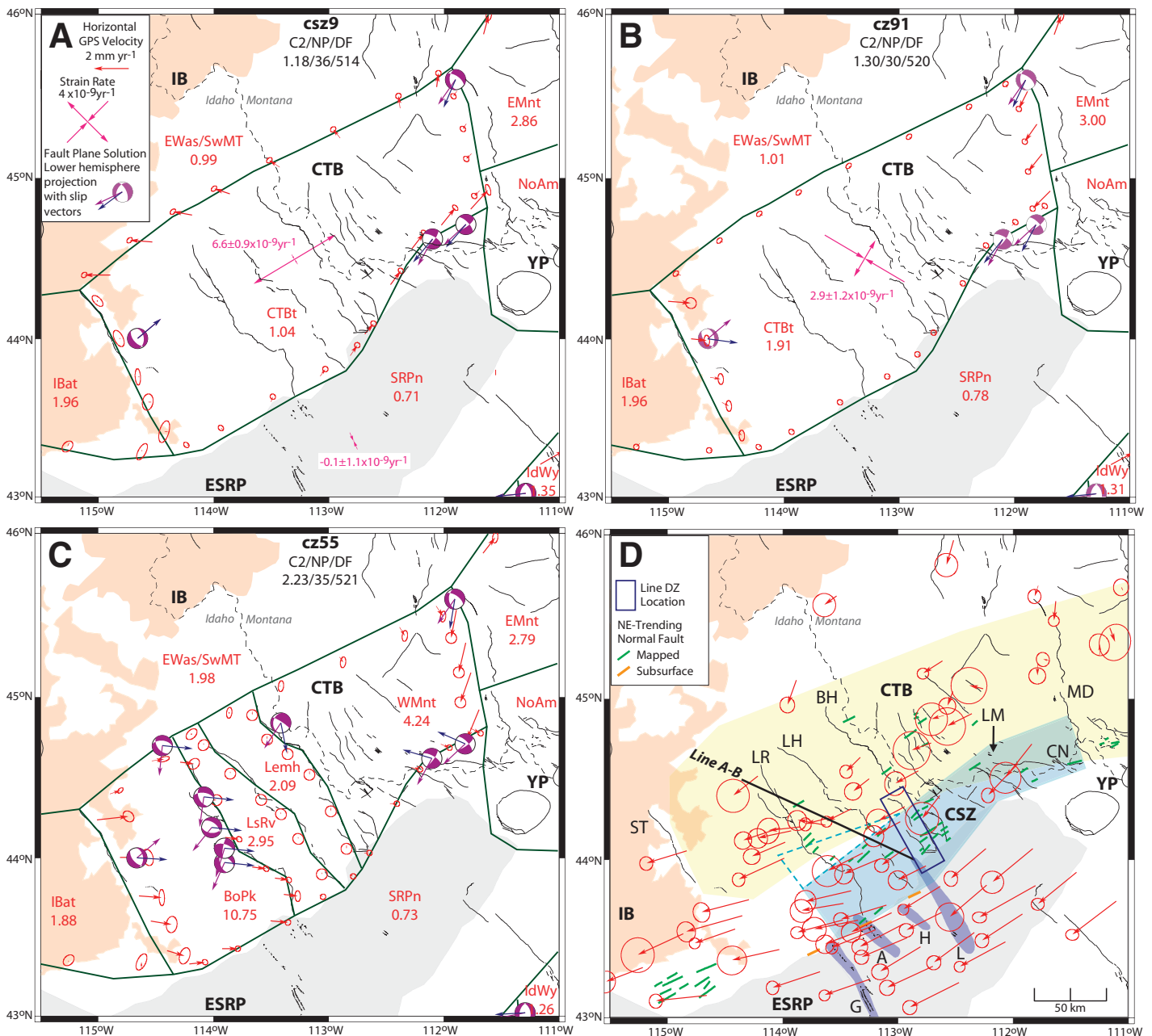


Figure 2. Maps showing results of inversions for models (A) cz29, (B) cz91, and (C) cz55 (see Table 1 for model descriptions). Fault slip vectors are shown by red arrows with 70% confidence ellipses for free-slipping (no locking) block boundaries (green lines). Tails of the red arrows are on the moving side of a block boundary. Lower-hemisphere fault plane solutions show slip vector azimuths (purple) compared with predicted slip vector azimuths (blue) (Table DR2; Fig. DR1; GSA Data Repository [see text footnote 1]). The model name is given above the inversion results, which are listed below as C2/NP/DF (C2 is reduced chi-square, NP is the number of free parameters, and DF is degrees of freedom). Each block is labeled with its name (red letters) and reduced chi-square (red number) fit of the velocities. Principal horizontal strain rates (pink arrows) are labeled with the extensional strain rate (pink letters). (D) Map showing 1994–2010 observed global positioning system (GPS) horizontal velocities (red vectors) and uncertainties (at 70% confidence ellipses) in the stable North American reference frame. “Line A-B” shows the location of the velocity profile for Figure 3B. Blue box shows the location for line DZ in Figure 4B. Shaded blue region and dashed lines (where inferred) show the boundaries of the Centennial shear zone interpreted in this study. Green lines show locations of mapped NE-trending faults, and orange lines show subsurface normal faults identified by geophysical data as presented in Figure 1B. See Figure 1 caption for abbreviations and references. Block labels: eastern Washington (EWAs), eastern Oregon (EOre), Idaho-Wyoming border (IdWy), Great Basin (GrBn), southwest Montana (SwMT), eastern Montana (EMnt), Idaho batholith (IBat), Centennial Tectonic Belt (CTB), Snake River Plain combined with the Owyhee-Oregon Plateau (SRPn), western Montana (WMnt), Lemhi (Lemh), Lost River (LsRv), and Borah Peak (BoPk).

TABLE 1. RESULTS OF MODEL MISFITS FOR INVERSIONS

Model	Tectonic model description	Model fit*		
		χ^2_{η}	NP	DOF
csz9	Different strain rates between the Centennial tectonic belt and eastern Snake River Plain.	1.18	36	514
cz91	No dextral strike-slip motion along boundaries and distributed oblique normal slip is accommodated by normal faults within the Centennial tectonic belt.	1.30	30	520
cz55	Block boundaries representing three NW-trending normal faults allow four blocks to rotate at rates of -0.50° to -0.55° m.y. $^{-1}$. Rates equivalent to producing a velocity of up to 1.4 mm yr $^{-1}$ over a 150 km fault length (or across the entire Centennial tectonic belt).	2.23	35	521
cz52	Block boundaries representing three NW-trending normal faults allow four blocks to rotate at rates of -0.20° to -0.25° m.y. $^{-1}$. Rates based on average paleomagnetic clockwise rotation of -10.3° since 47.7 to 49.3 Ma.	1.61	35	521
cz56	Block boundaries representing the three NW-trending normal faults allow four blocks to rotate at rates of -0.60° to -0.65° m.y. $^{-1}$. Rates based on average paleomagnetic clockwise rotation of -10.3° since 16 Ma.	2.35	35	521

* χ^2_{η} —reduced chi-square; NP—number of free parameters; DOF—degrees of freedom.

above, is negative). This range of rates is equivalent to producing a velocity change of ~ 1.4 mm yr $^{-1}$ over a 150 km block length (see GSA Data Repository for calculation [see footnote 1]). Model cz55 shows a very poor fit to the data ($\chi^2_{\eta} = 2.23$; Table 1) and predicts left-lateral oblique reverse slip rather than the observed oblique normal slip along the block-bounding faults (e.g., Lost River fault in Fig. 2C). Hence, we reject this model at $>99\%$ probability (Table 2) when compared to model csz9 ($\chi^2_{\eta} = 1.18$). In model cz52, we based rotation rates on Janecke et al. (1991), who reported paleomagnetic data for clockwise rotation at sites in middle Eocene volcanic rocks (47.7–49.3 Ma) within the southern Lost River and Lemhi mountain ranges. We used their data to estimate an average clockwise rotation of -10.3° , which corresponds to an average rotation rate of -0.21° m.y. $^{-1}$ over the past ~ 48 m.y. We also noted that west of the Lost River fault, a clockwise rotation of $-24^{\circ} \pm 5.7^{\circ}$ was measured in rocks estimated to be 51.1–65.3 Ma in age, which results in a range of potential rotation rates from -0.29° to -0.59° m.y. $^{-1}$, respectively (Latta, 2000; Anastasio et al., 2011). The faster rotation rate was already tested in model cz55 (Fig. 2C). Using lower rotation rates between -0.20° and -0.25° m.y. $^{-1}$ in model cz52, we again found a poor fit to the data ($\chi^2_{\eta} = 1.61$; Table 1) and rejected it at $>99\%$ probability (Table 2) when compared to model csz9 ($\chi^2_{\eta} = 1.18$; Fig. DR6 and GSA Data Repository [see footnote 1]). If instead, we assumed that Basin and Range faulting began ca. 16 Ma (Rodgers et al., 2002), then the average paleomagnetic clockwise rotation rate is -0.64° m.y. $^{-1}$ for the average clockwise rotation of -10.3° (based on Janecke et al., 1991). Constraining local clockwise rotation of each block to be within -0.60° to -0.65° m.y. $^{-1}$, we found model cz56 (Fig. DR7 and GSA Data Repository [see footnote 1]) also resulted in a very poor fit ($\chi^2_{\eta} = 2.35$; Table 1) and rejected it at $>99\%$ probability (Table 2). The results of these three tests show that the GPS and earthquake data do not at present support rapid rotation of the ranges within the Centennial tectonic belt.

We also evaluated the observed GPS velocities for the specific application of the model presented by McKenzie and Jackson (1986). According to the bookshelf model, slip on the faults should be perpendicular to the bounding shear zone. The slip vector azimuth for the fault plane solution of the 1983 M 6.9 Borah Peak, Idaho, earthquake is 204° (Richins et al.,

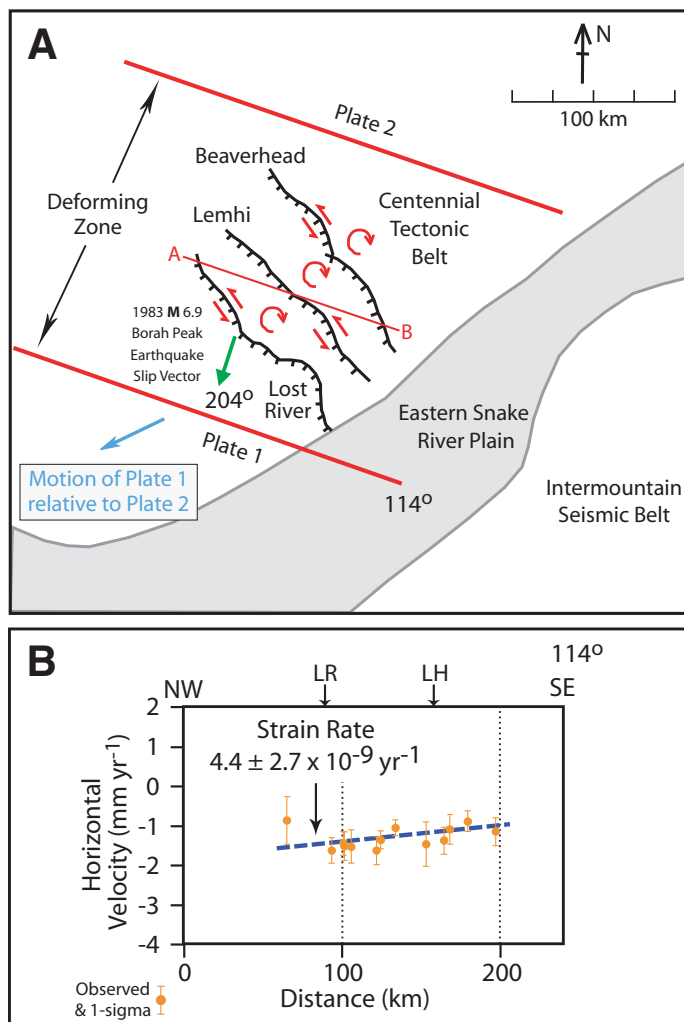


Figure 3. (A) Application of the “bookshelf” faulting model to the three NW-trending normal faults in the Centennial tectonic belt where the strike (114°) of the hypothetical plate boundaries and line A-B (red solid line) are oriented perpendicular to the slip vector (green arrow) of 204° (Richins et al., 1987) for the 1983 moment magnitude (M) 6.9 Borah Peak, Idaho, earthquake (figure modified from McKenzie and Jackson, 1986). Light-blue vector indicates direction of motion for plate 1 relative to plate 2. Semicircular red arrows show clockwise rotation of the ranges. Normal faults are shown by black lines and ticks on hanging wall. Red arrow pairs show oblique sense of motion on normal faults. See text for model discussion. (B) Profile shows components of observed horizontal velocities and one-sigma uncertainties parallel to the direction of the profile, which indicates extension for a positive slope. The strain rate and uncertainty (dashed blue line) were calculated in this study using a weighted least-square linear regression of velocities along the profile (Table DR1; GSA Data Repository [see text footnote 1]). Negative velocities indicate they are opposite in direction to the direction of the profile. The length of the dashed blue line corresponds to the length of line A-B on the map in Figure 2D. LH—Lemhi; LR—Lost River.

1987), which orients the strike azimuth at 114° for the bounding plates and line A-B across the normal faults (Fig. 3A). We projected components of the observed velocities parallel to the azimuth of 114° (Fig. 2D) and used a weighted least-squares linear regression to calculate the strain rate (Table DR1 and GSA Data Repository [see footnote 1]). The resulting extensional strain rate of $4.4 \pm 2.7 \times 10^{-9}$ yr $^{-1}$ (Fig. 3B) across the three

TABLE 2. RESULTS OF F-DISTRIBUTION TESTS FOR MODEL PAIRS

Model	χ_n^2	DOF	<i>P</i> (%)
csz9	1.18	514	90
cz91	1.30	520	
csz9	1.18	514	100
cz55	2.23	521	
csz9	1.18	514	100
cz52	1.61	521	
csz9	1.18	514	100
cz56	2.35	521	

Note: χ_n^2 —reduced chi-square; DOF—degrees of freedom; *P*—probability that misfit variances are from different distributions.

normal faults is not consistent with the McKenzie and Jackson (1983) model, which predicts no change in length along line A-B (Fig. 3A). From the four model tests and observed velocities, we conclude that modern-day GPS and earthquake data do not support a bookshelf style of faulting of the Centennial tectonic belt. Model csz9, with shear along the boundaries of the Centennial tectonic belt, fits the data better and indicates that right-lateral shear along the NE-trending boundary results from different strain rates in the Centennial tectonic belt and eastern Snake River Plain.

Gravitation Potential Energy Calculations

Since we concluded that normal faulting in the Centennial tectonic belt is not driven by shear stress at its boundaries, we explored whether lateral GPE variations might drive shear. To this end, we calculated and compared the GPE values for the Centennial tectonic belt and eastern Snake River Plain. We calculated GPE as the downward force per unit area exerted by a column of rock given by (Stüwe, 2002):

$$GPE = \int_h^z \rho g dz.$$

The rock density is expressed by ρ , the acceleration of gravity by g , depth below the surface by z , and the elevation above the surface defined at 0 by h . For all rock columns, the integration is performed to a depth of 50 km, below which there are no lateral density differences between the density models (Table 3). We used the ETOPO5 topographic data to assign elevations on a grid using a spacing of 0.2° for the region shown in Figure 4, and we used the same elevation grid for all density models listed in Table 3. GPE values were calculated at each grid point using the density column below the point and then smoothed using a moving-window low-pass filter to evaluate longer-wavelength features (filtering was applied to the GPE values to smooth the density models). We then calculated horizontal GPE gradients using the smoothed GPE values (see Figs. DR9–DR12 and GSA Data Repository [see footnote 1]).

We adopted distinct density models for the eastern Snake River Plain (SRP), Yellowstone Plateau (YST), the Basin and Range region southeast of the Snake River Plain (SBR), and Centennial tectonic belt (CTB) (Table 3). We included density models for the Yellowstone Plateau and southeast Basin and Range to allow calculations along the boundaries of the eastern Snake River Plain (Fig. 4). The density models and their regional boundaries are based on the recent modeling results of DeNosaquo et al. (2009). They suggest that crustal structures for the eastern Snake River Plain and Yellowstone Plateau (at Island Park; IP in Fig. 1B) include a midcrustal mafic sill with varying thickness and a 3-km-thick basal crustal underplated layer overlain by a 2-km-thick mafic partial melt at the base

TABLE 3. DENSITY MODELS USED TO CALCULATE GRAVITATIONAL POTENTIAL ENERGY (GPE)

Model [§]	Original*		Sill only [†]		Underplated only [†]	
	Thickness (km)	Density (kg/m ³)	Thickness (km)	Density (kg/m ³)	Thickness (km)	Density (kg/m ³)
CTB	6	2500	No changes		No changes	
	13	2670				
	20	3000				
	11	3300				
SBR	3	2500	No changes		No changes	
	16	2670				
	19	3000				
	12	3300				
YST	3	2500	3	2500	3	2500
	10	2670	10	2670	16	2670
	6	2820	6	2820	18	3000
	18	3000	20	3000	2	2850
	2	2850	11	3300	3	3200
	3	3200			8	3300
	8	3300				
SRP	1	2450	3	2500	3	2500
	2	2500	7	2670	17	2670
	7	2670	10	2900	17	3000
	10	2900	19	3000	2	2850
	17	3000	19	3300	3	3200
	2	2850			8	3300
	3	3200				
	8	3300				

*References for density models: CTB—Sheriff and Stickney (1984); Stickney (1997); DeNosaquo et al. (2009); SBR, YST, and SRP—DeNosaquo et al. (2009).
[†]Density models modified for this study.

[§]CTB—Centennial Tectonic Belt, SBR—Basin and Range region southeast of the Snake River Plain, YST—Yellowstone Plateau, SRP—eastern Snake River Plain.

of the crust (42 km). In our “original” set of density models (Table 3), we assumed that the sill below the eastern Snake River Plain has a constant thickness of 10 km starting at a depth of 10 km and assigned it a density of 2900 kg m⁻³ as per DeNosaquo et al. (2009). For the transitional sill in the YST density model (Table 3), we assumed a constant thickness of 6 km starting at a depth of 13 km and assigned it a density of 2820 kg m⁻³ as per DeNosaquo et al. (2009). In both the SRP and YST density models, the partial melt and underplated layers were assigned densities of 2850 and 3200 kg m⁻³, respectively (DeNosaquo et al., 2009). In contrast, the CTB and SBR density models did not include anomalous mid- or lower-crustal features. The density model for the SBR has upper-crustal (16-km-thick) and lower-crustal (19-km-thick) layers that are assigned densities of 2670 and 3000 kg m⁻³, respectively, and a total crustal thickness of 38 km (Table 3) based on DeNosaquo et al. (2009). The CTB density model has upper- and lower-crustal layers with densities of 2670 and 3000 kg m⁻³, respectively, also based on DeNosaquo et al. (2009). The upper- and lower-crustal thicknesses (13 and 20 km, respectively) along with the crustal thickness of 39 km (Table 3) are based on Sheriff and Stickney (1984) and Stickney (1997).

To assess the impacts on GPE of differences in topography and density models of the eastern Snake River Plain and Centennial tectonic belt, we calculated the GPE for three different sets of density models, “underplated only,” “sill only,” and “original” (Table 3). We recognize that the Centennial tectonic belt has relatively higher topographic relief than the eastern Snake River Plain, but the eastern Snake River Plain has a high-density midcrustal sill and a thickened crust with possible low-density layers (par-

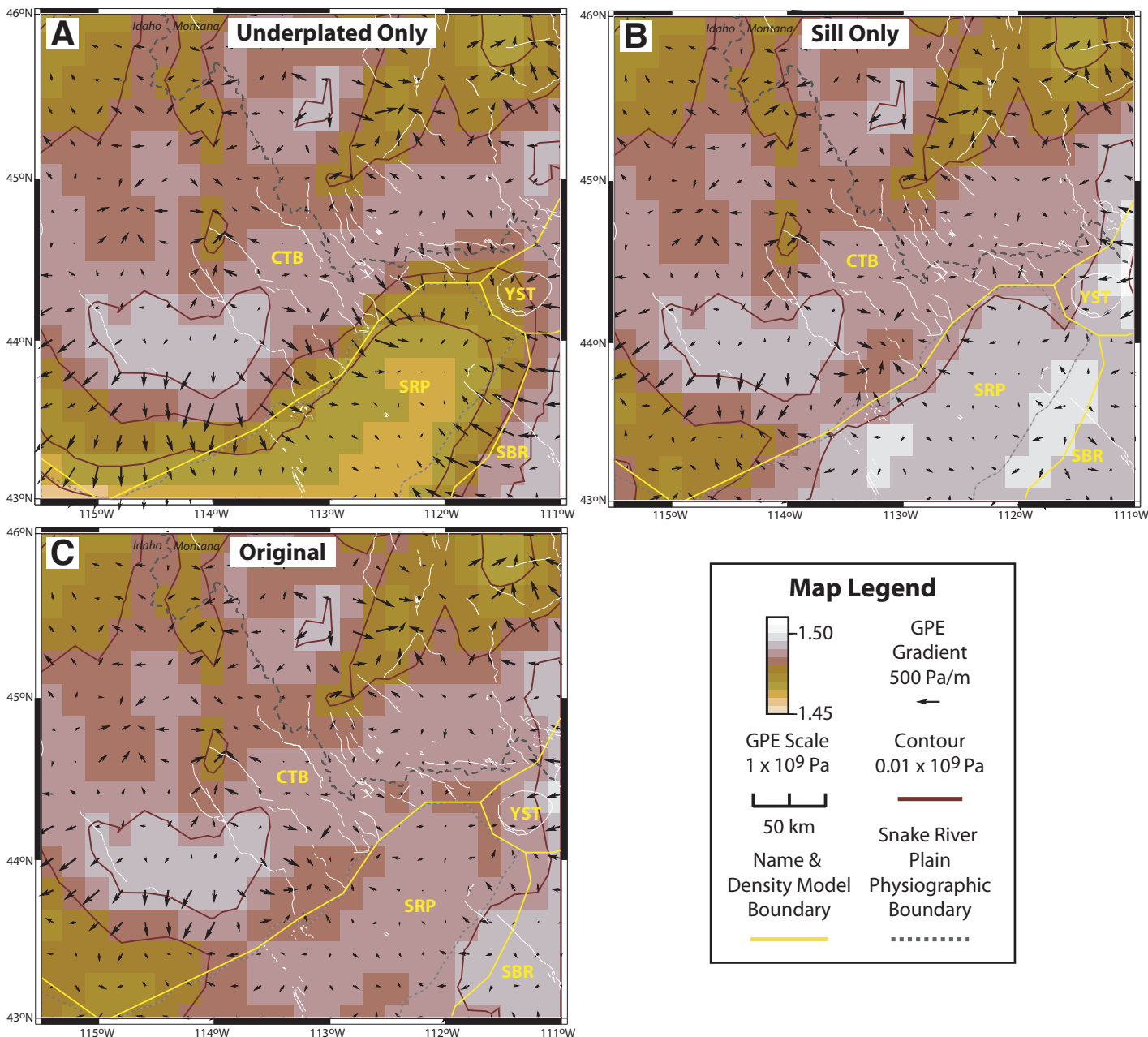


Figure 4. Maps showing gravitational potential energy (GPE) and gradients for density models: (A) “Underplated only” density models, which have the SRP and YST models modified to include only partial melt and underplated layers and maintaining a crustal thickness of 42 km; (B) “sill only” density models, which have the SRP and YST models modified to include only the midcrustal mafic sill and a crustal thickness of 39 km to match the CTB density model; and (C) “original” density models, including the SRP, YST, SBR, and CTB models as listed in Table 3. Gravitational potential energy variations and gradients were calculated using ETOPO5 topographic data set for 0.2° grid and density models listed in Table 3 (see text for details). Density models names: eastern Snake River Plain (SRP), Yellowstone Plateau (YST), Basin and Range region southeast of the Snake River Plain (SBR), and Centennial Tectonic Belt (CTB).

tial melt and underplated) not observed beneath the Centennial tectonic belt. To isolate impacts of each of these crustal perturbations to GPE estimates, we modified the SRP and YST “original” density models. The “underplated only” SRP and YST density models included the original densities for the underplated layers, the 42-km-thick crusts, and sill layer densities changed to 2670 kg m⁻³, which match the upper-crustal densities of the CTB model. The “sill only” SRP and YST density models included

the original densities of the sill layers, and, to match the CTB density model, densities of the lower-crustal layers were changed to 3000 kg m⁻³ and the total crustal thicknesses were set to 39 km. We did not change the CTB and SBR density models (Table 3). Results for the “underplated only” set of density models show lateral GPE variations primarily due to differences in topography. Figure 4A shows that the Centennial tectonic belt has generally higher GPE than the eastern Snake River Plain due to

higher topography, and the eastern Snake River Plain has more uniform, lower GPE due to generally lower-lying and flat topography (Fig. 1A). Moreover, GPE gradients in Figure 4A indicate a tendency for gravitational collapse of topography toward (or into) the eastern Snake River Plain. Alternatively in Figure 4B, use of the “sill only” density models shows that higher GPE in the eastern Snake River Plain is primarily due to the high-density sill layer, which is not present in the Centennial tectonic belt. Also, the sill layer extends beyond the southeast physiographic boundary of the eastern Snake River Plain (DeNosaquo et al., 2009), and thus, the higher relief coupled with the high-density sill layer result in even greater GPE in this region (Fig. 4B). The GPE gradients in Figure 4B are higher in the Centennial tectonic belt, showing the effects of larger differences in topography. Finally, in Figure 4C, use of the “original” density models shows that elevated GPE values due to the sill layer in the eastern Snake River Plain are somewhat similar to or less than the GPE in the Centennial tectonic belt, but the GPE gradients are higher in the Centennial tectonic belt than in the eastern Snake River Plain. Overall, Figure 4 shows that the Centennial tectonic belt has higher GPE values due to higher topography and a greater tendency for gravitational collapse of topography and that elevated GPE values in the low-lying Snake River Plain are due to the midcrustal sill layer (Figs. 4B and 4C). Comparisons of the GPE and gradients suggest that without the elevated GPE due to the midcrustal sill layer (Figs. 4B and 4C), gravitational collapse might occur into the eastern Snake River Plain (Fig. 4A).

DISCUSSION

Results of our GPS analyses indicate that right-lateral shear along the NW margin of the eastern Snake River Plain results from different strain rates in the eastern Snake River Plain and Centennial tectonic belt. GPE variations may in part explain the differences in strain rates since our results show higher GPE variations and a greater tendency for gravitational collapse in the Centennial tectonic belt as opposed to the lower GPE variations in the eastern Snake River Plain. We integrated our modeling results with geological, geophysical, and seismological data to: (1) interpret that extension in the Centennial tectonic belt drives right-lateral shear; (2) propose boundaries for and suggest mechanisms of deformation within the Centennial shear zone; and (3) offer examples of locations where right-lateral shear may be accommodated within the Centennial shear zone.

Extension-Driven Shear

Results of our kinematic GPS analyses suggest that right-lateral shear along the NE-trending boundary results from different strain rates in the Centennial tectonic belt ($6.6 \pm 0.9 \times 10^{-9} \text{ yr}^{-1}$) and eastern Snake River Plain ($-0.1 \pm 1.1 \times 10^{-9} \text{ yr}^{-1}$, which is effectively zero; Fig. 2A). Based on kinematic modeling of GPS and paleomagnetic data, bookshelf faulting, in which right-lateral shear along the NW boundary of the eastern Snake River Plain drives normal faulting over the entire Centennial tectonic belt, is not a viable model. The contrasting strain rates may be caused by differences in internal differential stress acting upon the Snake River Plain and the Centennial tectonic belt, or differences in lithospheric strength, or both. Differential stress variations could result from differences in GPE variations within these regions. Humphreys and Coblenz (2007) proposed that GPE-derived stress contributes to driving extensional orogenic collapse in the western United States. Our results in Figure 4 show that GPE variations could drive gravitational collapse at a higher rate in the higher topographic relief in the Centennial tectonic belt outside of the eastern Snake River Plain. Alternatively, the eastern Snake River Plain has more

uniform, lower GPE variations due to its relatively flat topography and higher-density crustal composition from the mafic sill layer. We suggest that the low GPE variations in the eastern Snake River Plain may in part explain its lower rate of deformation relative to the surrounding Basin and Range. Also from Figure 4C, we propose that the dense mafic sill increases GPE in the eastern Snake River Plain and offsets the greater GPE of the Centennial tectonic belt due to its higher topography, thus preventing gravitational collapse into the eastern Snake River Plain (Fig. 4A). We observe that the GPS velocities show no extension of the Centennial tectonic belt toward the eastern Snake River Plain (Fig. 2A).

To see the differences more clearly in the GPS observations, we rotated the velocities into a “Snake River Plain” frame of reference using the angular velocity of the SRPn block from model csz9. Divergent velocities within the Centennial tectonic belt indicate extension at a much higher rate than in the eastern Snake River Plain (Fig. 5A). Relative to the slowly deforming eastern Snake River Plain region, the Centennial

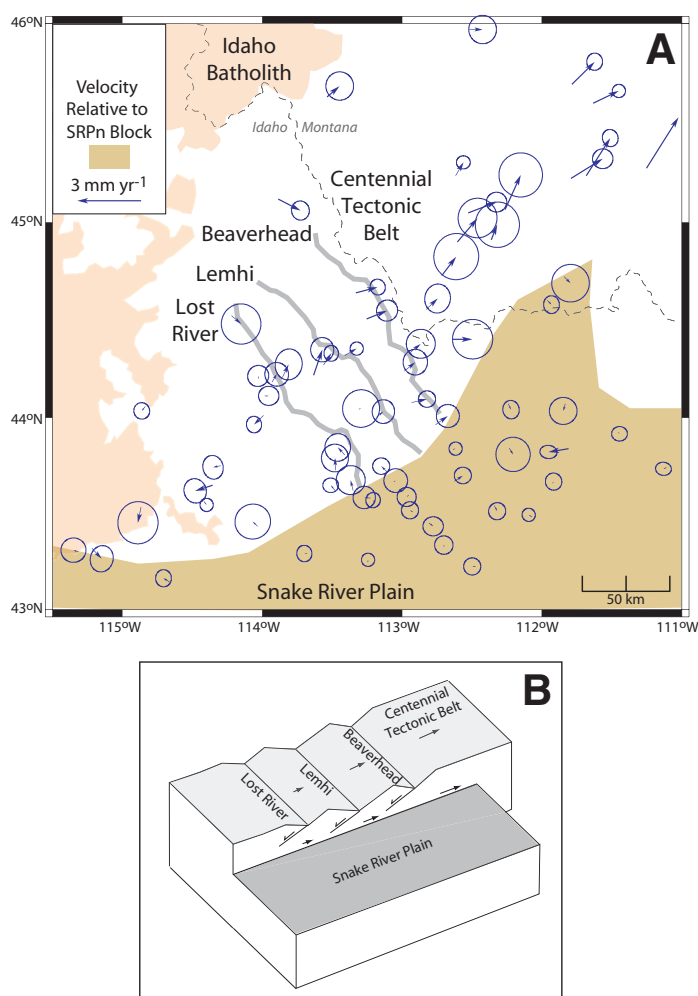


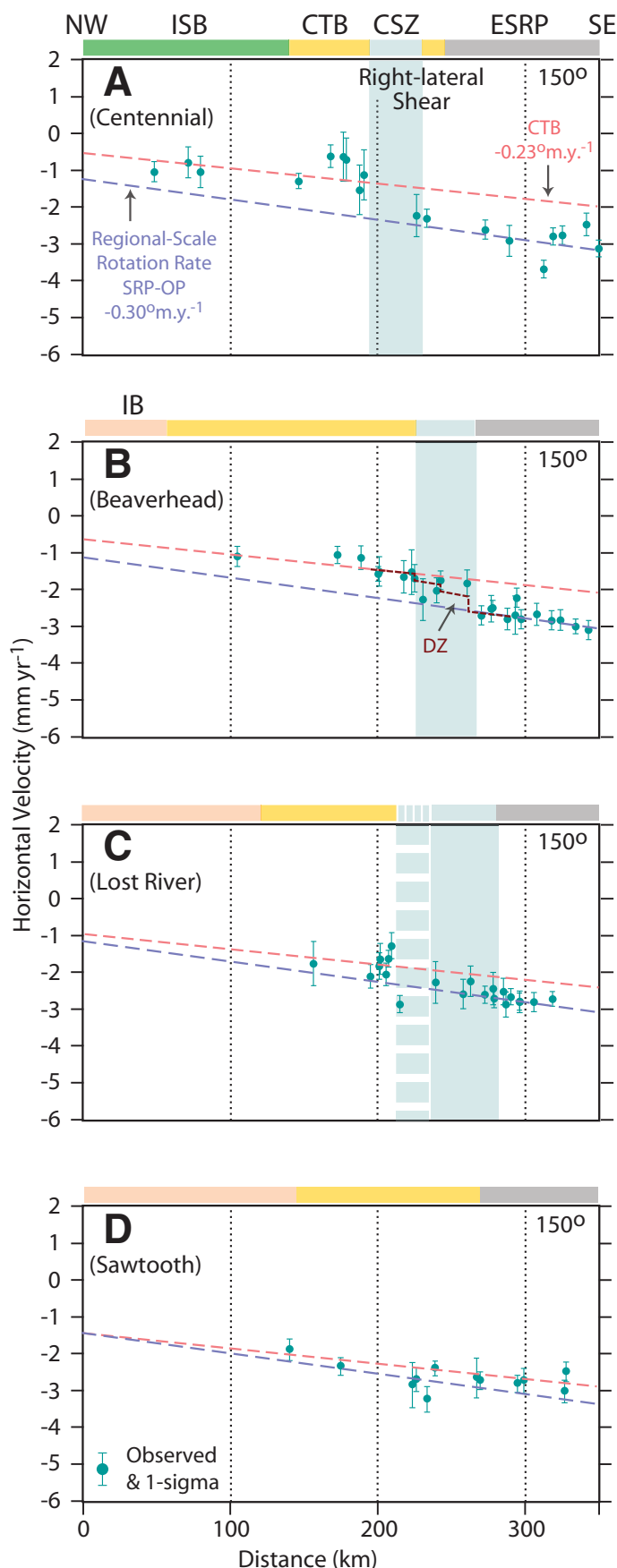
Figure 5. (A) Map showing horizontal velocities rotated into a Snake River Plain (SRPn) frame of reference using the angular velocity of the SRPn block (Snake River Plain and Owyhee-Oregon Plateau) from model csz9 (Fig. DR8; GSA Data Repository [see text footnote 1]). Velocities are shown by blue arrows and 70% confidence ellipses. (B) Block diagram showing the NE direction of motion of the extending Centennial tectonic belt with respect to the Snake River Plain, which results in right-lateral shear along the boundary between the two provinces.

tectonic belt is rapidly extending to the northeast, which we suggest is due to gravitational collapse, and we further suggest that this extension drives right-lateral shear (Fig. 5B).

Shear Accommodation in the Centennial Shear Zone

We suggest that the differential motion between the Centennial tectonic belt and eastern Snake River Plain is likely distributed across the Centennial shear zone rather than concentrated along any discrete fault. Model *csz9* predicts rates of right-lateral strike-slip motions that vary from 0.3 mm yr^{-1} near the southeast end of the Lost River fault to 1.5 mm yr^{-1} near Centennial fault (Fig. 2A). In the block model, we represent this NE-trending slipping boundary as a localized discrete fault, but we understand that the NW boundary of the eastern Snake River Plain lacks recognizable strike-slip faults (e.g., Kuntz et al., 1994; Rodgers et al., 2002; Holmes et al., 2008). In Figure 6, we show four NW-SE profiles with components of the velocities perpendicular to the direction of the profiles encompassing the Centennial tectonic belt and eastern Snake River Plain (0–350 km). The observed velocities in all four profiles exhibit negative slopes that indicate either clockwise rotation or right-lateral shear or both. From their evaluation of the observed velocities, Payne et al. (2012) estimated regional-scale rotation rates for the Centennial tectonic belt ($-0.23^\circ \text{ m.y.}^{-1}$) and Snake River Plain–Owyhee-Oregon Plateau region ($-0.30^\circ \text{ m.y.}^{-1}$) (see their fig. 10), which are interpreted as part of the larger-scale rotation rates over the Pacific Northwest (McCaffrey et al., 2007, 2013). For each profile in Figure 6, we plotted two lines with negative slopes equivalent to rotation rates of $-0.23^\circ \text{ m.y.}^{-1}$ and $-0.30^\circ \text{ m.y.}^{-1}$ and aligned each slope with the velocities in their respective tectonic provinces. Profiles across the Centennial fault (Fig. 6A) and along the Beaverhead fault (Fig. 6B) show that between the expected gradients in the velocity field for the two rotation rates, there are additional downward steps in the observed velocities, which we interpret as narrower bands of right-lateral shear (35 and 40 km wide, respectively). The profile along the Lost River fault shows a smaller downward step that could be 45 or 80 km wide, depending on whether or not we include the velocity at the 212 km distance (Fig. 6C). The profile along the Sawtooth fault does not show an obvious step, and we do not see a zone of right-lateral shear (Fig. 6D). We interpolated between the narrow bands of right-lateral shear shown by the blue shaded regions of the profiles in Figure 6 to define the boundaries of the Centennial shear zone. We suggest that the zone spans a NE-trending, 40–45-km-wide zone along NW boundary of the eastern Snake River Plain from the Centennial to the Beaverhead fault

Figure 6. (A–D) Profiles showing components of observed horizontal velocities and one-sigma uncertainties perpendicular to the direction of the profile, which indicate clockwise rotation or right-lateral shear or both for negative slopes. Negative velocities indicate they are opposite in direction to the direction of the profile. Regional-scale rotation rates of $-0.23^\circ \text{ m.y.}^{-1}$ for the Centennial tectonic belt (dashed light red line) and $-0.30^\circ \text{ m.y.}^{-1}$ for Snake River Plain combined with the Owyhee-Oregon Plateau (dashed light blue line) estimated by Payne et al. (2012) are shown on each profile. Line “DZ” (dashed brown line) exhibits how right-lateral shear could be accommodated within the Centennial shear zone (see text for further explanation). Color bar along the top indicates tectonic provinces along profiles shown in Figure 1A. CTB—Centennial tectonic belt (Stickney and Bartholomew, 1987); CSZ—Centennial shear zone; ESRP—eastern Snake River Plain; IB—Idaho Batholith (Bond et al., 1978; Stoesser et al., 2005); ISB—Intermountain Seismic Belt (Smith and Arabasz, 1991); OP—Owyhee-Oregon Plateau; SRP—Snake River Plain.



and that it may widen to 80 km near the Lost River fault, but that it is not well defined near the Sawtooth fault, if present at all (Fig. 2D).

The distributed differential motion across the Centennial shear zone could have components of deformation due to regional-scale rotation, strike-slip faulting, and distributed simple shear or some combination of these. The velocity (or downward) steps in the profiles that define the Centennial shear zone include a component of regional-scale rotation along with deformation that may be observed as strike-slip faulting along E- and NE-trending faults or left-lateral oblique slip along NW-trending faults for bookshelf faulting on a very local scale within the Centennial shear zone (i.e., distributed simple shear). As an example only for the Beaverhead fault profile shown in Figure 6B, we illustrate how the Centennial shear zone could accommodate a combination of rotation and faulting by using the brown dashed line labeled “DZ” through the observed velocities. The vertical steps of the line DZ would be the locations where right-lateral shear is accommodated by strike-slip motion on discrete NE-trending faults (blue box in Fig. 2D). Line DZ decreases in slope from the NW to the SE to match up with the two regional-scale rotation rates of -0.23° and $-0.30^\circ \text{ m.y.}^{-1}$, respectively (Fig. 6B).

We offer some geologic examples of where and how distributed strike-slip and simple shear deformation could occur within the Centennial shear zone. The NE-trending normal faults in the mountain ranges adjacent to the three NW-trending normal faults (e.g., Zentner, 1989; Janecke, 1992; Rodgers et al., 2002) are observed within the Centennial shear zone (green lines in Fig. 1B). While not necessarily optimally aligned, we suggest that these NE-trending normal faults and others nearby could be locations where right-lateral strike slip is accommodated. Also along the Snake River Plain’s physiographic boundary, the presumably NE-trending normal faults identified in the subsurface (Sparlin et al., 1982; Pankratz and Ackerman, 1982; Stanley, 1982) could accommodate right-lateral strike-slip motion (red lines in Fig. 1B). Bedrock structural features suggest that significant seismogenic fault movements do not extend into the eastern Snake River Plain and that perhaps the three normal faults (Lost River, Lemhi, and Beaverhead) terminate here. Near the southern end of the Lemhi fault, Bruhn et al. (1992) interpreted NE-striking cross faults associated with an asymmetrical NE-trending graben in the footwall of the Lemhi fault (blue box labeled LG in Fig. 1B) to accommodate differential motion over the past 4 m.y. between the Lemhi range and eastern Snake River Plain. Our GPS-derived strain rate estimates are consistent with the inference of Bruhn et al. (1992) and support the idea that slip on cross faults along the NW edge of the eastern Snake River Plain accommodates different rates of deformation between the Centennial tectonic belt and eastern Snake River Plain. Finally, right-lateral shear may be accommodated at the southern ends of NW-trending Centennial tectonic belt normal faults where they may project beneath the basalt cover of the eastern Snake River Plain (box labeled LF in Fig. 1B). The short, NW-trending normal faults and monoclin flexures within basalt flows have a generally left-stepping, en echelon pattern in a NE direction from the projection of the southern end of the Lost River fault into the eastern Snake River Plain (Kuntz et al., 1994). Monoclines in the basalt flows may be surface expressions of subsurface normal faults that have not breached the surface and are caused by flexure of the surface above upward-propagating fault tips (Grant and Kattenhorn, 2004). If tectonic in origin, the NW-trending normal faults are optimally aligned to accommodate right-lateral shear through components of left-lateral oblique slip (e.g., Clifton et al., 2000), which could indicate localized bookshelf faulting confined within the Centennial shear zone at this location (box labeled LF in Fig. 1B). Due to the low strain rate within the eastern Snake River Plain (Fig. 2A), the slip rates on these features would be much lower than slip rates of Lost River fault segments to the NW in the Centennial tectonic belt.

The highest rates of right-lateral strike-slip motions predicted from model csz9 are located near the Lima Reservoir and Centennial faults, which provide supporting geologic and seismological evidence of right-lateral shear (Fig. 7). The series of NW-trending, left-stepping, en echelon segments of the Centennial fault have ruptures as recent as mid- to late Pleistocene and are consistent with distributed dextral displacements during fault linkage (Petrik, 2008). The Lima Reservoir fault overlaps with the western end of the Centennial fault and also includes left-stepping segments thought to be consistent with accommodation of right-lateral shear (Majerowicz et al., 2007; Majerowicz, 2008; Anastasio et al., 2010). The Lima Reservoir fault has mid-Pleistocene to Holocene slip along its segments (Bartholomew et al., 2002; Anastasio et al., 2010). Also near these two faults, fault plane solutions within a NE-trending zone of seismicity are observed with strike-slip components of motion consistent with right-lateral shear (Fig. 7) (Stickney, 1997, 2007). Here, strike-slip earthquakes may occur on NE-trending faults parallel to our proposed boundary between the eastern Snake River Plain and Centennial shear zone (Fig. 2A). These observations extend the Centennial shear zone farther east beyond the Centennial fault profile (Fig. 6A) to include the NE-trending zone of seismicity and eastern end of the Centennial fault (Figs. 1B and 3D).

One possible explanation for the existence of the Centennial shear zone is that it serves as a transition zone necessary to accommodate right-lateral shear between the rapid extension in the Centennial tectonic belt and the slowly deforming eastern Snake River Plain. The GPS data indicate that at present there are differences in strain rates between these two regions, resulting in right-lateral shear. Slip along the Lima Reservoir and Centennial normal faults suggests that accommodation of right-lateral shear may have occurred over a longer period of time, perhaps since the mid-Pleistocene (Bartholomew et al., 2002; Anastasio et al., 2010) and possibly since 2 Ma, when slip initiated on the Centennial fault (Petrik, 2008).

CONCLUSIONS

From GPS and earthquake data, we conclude that boundary shear stress does not drive normal faulting across the entire Centennial tectonic belt. Our data indicate that oblique slip produced during the 1983 M 6.9 Borah Peak, Idaho, earthquake was not due to bookshelf style faulting as suggested by the model of McKenzie and Jackson (1983, 1986). Paleomagnetic and GPS data also do not reveal rates high enough for clockwise rotation of the Lost River, Lemhi, and Beaverhead ranges to support the bookshelf model. Conversely, our results indicate that rapid extension due to gravitational collapse within the Centennial tectonic belt ($6.6 \pm 0.9 \times 10^{-9} \text{ yr}^{-1}$) juxtaposed against the low-deforming eastern Snake River Plain ($-0.1 \pm 1.1 \times 10^{-9} \text{ yr}^{-1}$, not resolvable from zero) drives right-lateral shear between the two regions. GPE calculations suggest the presence of higher variations within the Centennial tectonic belt due to higher topography and more uniform and smaller GPE variations within the eastern Snake River Plain due to flat topography and a denser crustal composition. The low GPE variations in the eastern Snake River Plain may in part explain its lower rate of deformation. Our GPE results also suggest that the dense mafic sill elevates GPE values in the eastern Snake River Plain, making them similar to the GPE values in the Centennial tectonic belt, which prevents gravitational collapse of the Centennial tectonic belt into the eastern Snake River Plain.

We suggest that the Centennial shear zone spans a NE-trending, 40–45-km-wide zone along the NW boundary of the eastern Snake River Plain from the Centennial fault to the Beaverhead fault, and it may then widen to 80 km near the Lost River fault. Within the zone of shear, the GPS data support the interpretation that differential motion is distributed and may reflect components of deformation due to strike-slip faulting, dis-

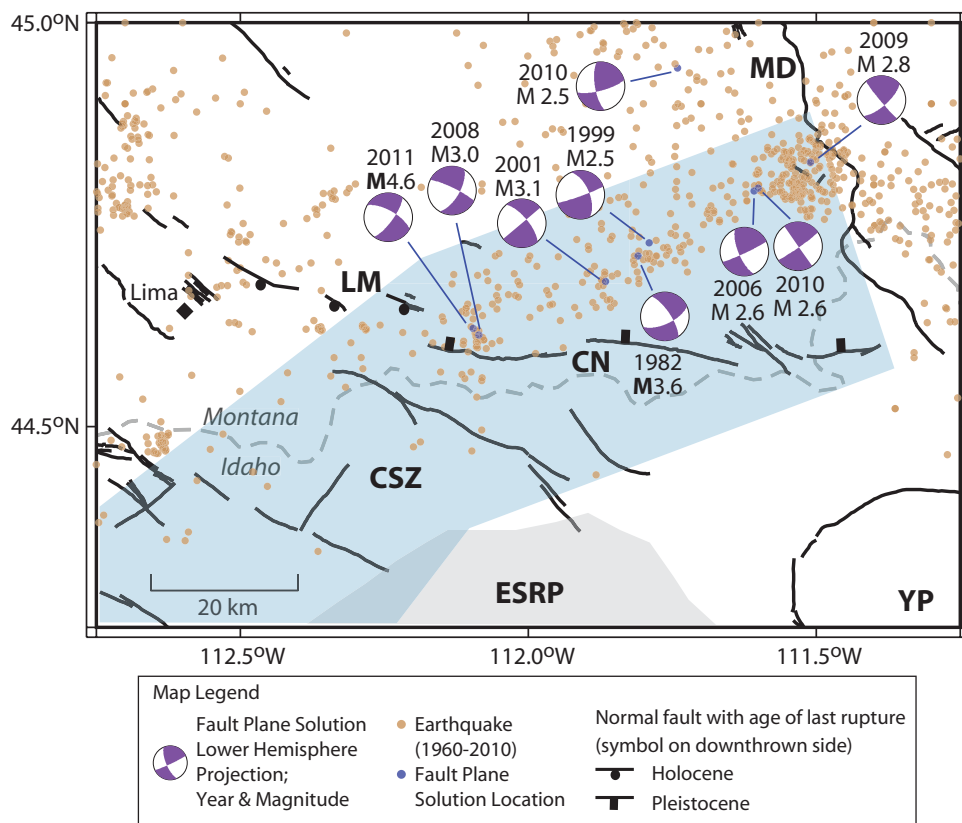


Figure 7. Map showing locations of lower-hemisphere fault plane solutions with components of strike-slip motion and ages of last ruptures along the Centennial (CN) and Lima Reservoir (LM) faults within the Centennial shear zone (CSZ). Fault plane solutions have year and magnitude (coda or local magnitude for M; moment magnitude for M) and are unpublished data courtesy of the Montana Bureau of Mines and Geology (Table DR3; GSA Data Repository [see text footnote 1]). Earthquake epicenters (brown dots) were compiled for magnitudes greater than 2.0 from 1960 to 2011 (Advanced National Seismic System, 2011), and blue dots indicate locations of fault plane solutions. Ages of last ruptures for the Lima Reservoir fault are from Bartholomew et al. (2002), Anastasio et al. (2011), D. Anastasio (2013, personal commun.), and those for the Centennial fault are from Petrik (2008). See Figure 1 caption for other abbreviations. ESRP—eastern Snake River Plain; MD—Madision fault; and YP—Yellowstone Plateau.

tributed simple shear, regional-scale rotation, or some combination of these. We propose that right-lateral strike slip may be accommodated along existing mapped NE-trending normal faults within the Centennial shear zone and possible subsurface faults interpreted in geophysical data along the NW physiographic boundary of the eastern Snake River Plain. Moreover, we suggest that the southernmost ends of NW-trending Centennial tectonic belt faults at their juncture with the eastern Snake River Plain could also accommodate right-lateral shear through components of left-lateral oblique slip as localized bookshelf faulting. Finally, where the GPS data indicate the largest rates of right-lateral strike-slip motions near the Centennial fault, we observe focal mechanisms with strike-slip components of motion consistent with right-lateral shear within a NE-trending zone of seismicity. Slip on the Lima Reservoir and Centennial normal faults also suggests accommodation of right-lateral shear during the Holocene and mid- to late Pleistocene.

ACKNOWLEDGMENTS

We very much appreciate the reviews by David Anastasio, Eric Kirby, and an anonymous reviewer, which helped improve the manuscript. We thank Bob King for his support and processing of the global positioning system data used in the study. We also thank Mike Stickney for providing us with fault plane solutions from the unpublished Montana Bureau of Mines and Geology catalog. Payne appreciates the helpful discussions and reviews by Seth Carpenter. The research was funded in part by the Idaho National Laboratory through the U.S. Department of Energy Idaho Operations Office contract DE-AC07-05ID14517. The research was supported by the National Earthquake Hazards Research Program (NEHRP) grant 2010-0006 and National Science Foundation (NSF) grant EAR-1062251 to McCaffrey.

REFERENCES CITED

- Advanced National Seismic System, 2011, ANSS Catalog Search: <http://www.ncedc.org/anss/catalog-search.html> (accessed January 2011).
- Anastasio, D.J., Majerowicz, C.N., Pazzaglia, F.J., and Regalla, C.A., 2010, Late Pleistocene–Holocene ruptures of the Lima Reservoir fault, SW Montana: *Journal of Structural Geology*, v. 32, p. 1996–2008, doi:10.1016/j.jsg.2010.08.012.
- Anastasio, D.J., Latta, D., Kodama, K.P., and Idleman, B.D., 2011, Thrusting rates in the early Eocene from the Sevier hinterland, Idaho, USA: *Washington, D.C., American Geophysical Union, Fall Meeting 2011*, abstract T51B–2335.
- Bartholomew, M.J., Stickney, M.C., Wilde, E.M., and Dundas, R.G., 2002, Late Quaternary paleoseismites: Syndepositional features and section restoration used to indicate paleoseismicity and stress-field orientations during faulting along the main Lima Reservoir fault, southwestern Montana, in Etensohn, R.F., Rast, N., and Brett, C.E., eds., *Ancient Seismites: Geological Society of America Special Paper 359*, p. 29–47.
- Bond, J.G., Kauffman, J.D., Miller, D.A., and Venkatakrishnan, R., 1978, *Geologic Map of Idaho: Moscow, Idaho, Idaho Bureau of Mines and Geology Map GM-1*, scale 1:500,000, 1 sheet.
- Bruhn, R.L., Wu, D., and Lee, J.-J., 1992, *Final Report on the Structure of the Southern Lemhi and Arco Fault Zone, Idaho: Idaho Falls, Idaho, EG&G Informal Report, EGG-NPR-10680*, 26 p.
- Chadwick, J.D., Rodgers, D.W., and Payne, S.P., 2007, Contemporary tectonic motion of the eastern Snake River Plain, Idaho: A global positioning system study, 1995–2004: *Tectonics*, v. 26, TC6005, doi:10.1029/2005TC001914.
- Clifton, A.E., Schlische, R.W., Withjack, M.O., and Ackermann, R.V., 2000, Influence of rift obliquity on fault-population systematics: Results of experimental clay models: *Journal of Structural Geology*, v. 22, p. 1491–1509, doi:10.1016/S0191-8141(00)00043-2.
- Crone, A.J., Machette, M.N., Bonilla, M.G., Lienkaemper, J.J., Pierce, K.L., Scott, W.E., and Bucknam, R.C., 1987, Surface faulting accompanying the Borah Peak earthquake and segmentation of the Lost River fault, central Idaho: *Bulletin of the Seismological Society of America*, v. 77, p. 739–770.
- DeNosaquo, K.R., Smith, R.B., and Lowry, A.R., 2009, Density and lithospheric strength models of the Yellowstone–Snake River Plain volcanic system from gravity and heat flow data: *Journal of Volcanology and Geothermal Research*, v. 188, p. 108–127, doi:10.1016/j.jvolgeores.2009.08.006.
- Elbring, G.J., 1984, *A Method for Inversion of Two-Dimensional Seismic Refraction Data with Applications to the Snake River Plain Region, Idaho* [M.S. thesis]: Salt Lake City, Utah, University of Utah, 123 p.
- Grant, J.V., and Kattenhorn, S.A., 2004, Evolution of vertical faults at an extensional plate boundary, southwest Iceland: *Journal of Structural Geology*, v. 26, p. 537–557, doi:10.1016/j.jsg.2003.07.003.
- Herrmann, R.B., Benz, H., and Ammon, C.J., 2011, Monitoring the earthquake source process in North America: *Bulletin of the Seismological Society of America*, v. 101, p. 2609–2625, doi:10.1785/0120110095.
- Holmes, A.A.J., Rodgers, D.W., and Hughes, S.S., 2008, Kinematic analysis of fractures in the Great Rift, Idaho: Implications for subsurface dike geometry, crustal extension, and magma dynamics: *Journal of Geophysical Research*, v. 113, B04202, doi:10.1029/2006JB004782.

- Humphreys, E.D., and Coblenz, D.D., 2007, North American dynamics and western U.S. tectonics: *Reviews of Geophysics*, v. 45, RG3001, doi:10.1029/2005RG000181.
- Jackson, S.M., Carpenter, G.S., Smith, R.P., and Casper, J.L., 2006, Seismic Reflection Project near the Southern Terminations of the Lost River and Lemhi Faults, Eastern Snake River Plain, Idaho: Idaho Falls, Idaho, Battelle Energy Alliance, INL/EXT-06-11851, 16 p.
- Janecke, S.U., 1992, Kinematics and timing of three superimposed extensional systems, east central Idaho: Evidence for an Eocene tectonic transition: *Tectonics*, v. 11, p. 1121–1138, doi:10.1029/92TC00334.
- Janecke, S.U., Geissman, J.W., and Bruhn, R.L., 1991, Localized rotation during Paleogene extension in east central Idaho: Paleomagnetic and geologic evidence: *Tectonics*, v. 10, p. 403–432, doi:10.1029/90TC02465.
- Kirkham, V.R.D., 1931, Snake River downwarp: *The Journal of Geology*, v. 39, p. 456–482, doi:10.1086/623864.
- Kuntz, M.A., Spiker, E.C., Rubin, M., Champion, D.E., and Lefebvre, R.H., 1986, Radiocarbon studies of latest Pleistocene and Holocene lava flows of the Snake River Plain, Idaho: Data, lessons, interpretations: *Quaternary Research*, v. 25, p. 163–176, doi:10.1016/0033-5894(86)90054-2.
- Kuntz, M.A., Covington, H.R., and Schorr, L.J., 1992, An overview of basaltic volcanism of the eastern Snake River Plain, Idaho, in Link, P.K., Kuntz, M.A., and Platt, L.B., eds., *Regional Geology of Eastern Idaho and Western Wyoming*: Geological Society of America Memoir 179, p. 227–267.
- Kuntz, M.A., Skipp, B., Lanphere, M.A., Scott, W.E., Pierce, K.L., Dalrymple, G.B., Champion, D.E., Embree, G.F., Page, W.R., Morgan, L.A., Smith, R.P., Hackett, W.R., and Rodgers, D.W., 1994, Geologic Map of the Idaho National Engineering Laboratory and Adjoining Areas, Eastern Idaho: U.S. Geological Survey Miscellaneous Investigation Map I-2330, 1:100,000 scale, 1 sheet.
- Kuntz, M.A., Anderson, S.R., Champion, D.E., Lanphere, M.A., and Grunwald, D.J., 2002, Tension cracks, eruptive fissures, dike, and faults related to late Pleistocene–Holocene basaltic volcanism and implications for the distribution of hydraulic conductivity in the eastern Snake River Plain, Idaho, in Link, P.K., and Mink, L.L., eds., *Geology, Hydrology, and Environmental Remediation: Idaho National Engineering and Environmental Laboratory, Eastern Snake River Plain, Idaho*: Geological Society of America Special Paper 353, p. 111–133.
- Latta, D.K., 2000, Out-of-Sequence Emergent Thrusting during the Early Tertiary, within the Sevier Hinterland, Montana Recess, South Central Idaho [M.S. thesis]: Bethlehem, Pennsylvania, Lehigh University, 54 p.
- Mabey, D.R., 1978, Regional gravity and magnetic anomalies in the eastern Snake River Plain: Idaho: U.S. Geological Survey Journal of Research, v. 6, p. 553–562.
- Majerowicz, C.N., 2008, Quaternary Rupture History of the Lima Reservoir Fault System, SW Montana [M.S. thesis]: Bethlehem, Pennsylvania, Lehigh University, 49 p., 1 plate.
- Majerowicz, C.N., Harkins, N.W., Regalla, C.A., Troy, J.K., Pazzaglia, F.J., and Anastasio, D.J., 2007, Transension along the northeastern boundary of the Snake River Plain: *Geological Society of America Abstracts with Programs*, v. 39, no. 6, p. 292.
- McCaffrey, R., 2009, Time-dependent inversion of three-component continuous GPS for steady and transient sources in northern Cascadia: *Geophysical Research Letters*, v. 36, p. L07304, doi:10.1029/2008GL036784.
- McCaffrey, R., Qamar, A.I., King, R.W., Wells, R., Khazaradze, G., Williams, C.A., Stevens, C.W., Vollick, J.J., and Zwick, P.C., 2007, Fault locking, block rotation and crustal deformation in the Pacific Northwest: *Geophysical Journal International*, v. 169, p. 1315–1340, doi:10.1111/j.1365-246X.2007.03371.x.
- McCaffrey, R., King, R.W., Payne, S.J., and Lancaster, M., 2013, Active tectonics of northwestern US inferred from GPS-derived surface velocities: *Journal of Geophysical Research*, v. 118, p. 1–15, doi:10.1029/2012JB009473.
- McKenzie, D., and Jackson, J., 1983, The relationship between strain rates, crustal thickening, paleomagnetism, finite strain and fault movements within a deforming zone: *Earth and Planetary Science Letters*, v. 65, p. 182–202, doi:10.1016/0012-821X(83)90198-X.
- McKenzie, D., and Jackson, J., 1986, A block model of distributed deformation by faulting: *Journal of the Geological Society of London*, v. 143, p. 349–353, doi:10.1144/gsjgs.143.2.0349.
- McQuarrie, N., and Rodgers, D.W., 1998, Subsidence of a volcanic basin by flexure and lower crustal flow: The eastern Snake River Plain, Idaho: *Tectonics*, v. 17, p. 203–220, doi:10.1029/97TC03762.
- Morgan, L.A., and McIntosh, W.C., 2005, Timing and development of the Heise volcanic field, Snake River Plain, Idaho, western USA: *Geological Society of America Bulletin*, v. 117, p. 288–306, doi:10.1130/B25519.1.
- Pankratz, L.W., and Ackerman, H.D., 1982, Structure along the northwest edge of the Snake River Plain interpreted from seismic refraction: *Journal of Geophysical Research*, v. 87, p. 2676–2682, doi:10.1029/JB087iB04p02676.
- Parsons, T., Thompson, G.A., and Smith, R.P., 1998, More than one way to stretch: A tectonic model for extension along the track of the Yellowstone hotspot and adjacent Basin and Range Province: *Tectonics*, v. 17, p. 221–234, doi:10.1029/98TC00463.
- Payne, S.J., McCaffrey, R., and King, R.W., 2008, Strain rates and contemporary deformation in the Snake River Plain and surrounding Basin and Range from GPS and seismicity: *Geology*, v. 36, p. 647–650, doi:10.1130/G25039A.1.
- Payne, S.J., McCaffrey, R., King, R.W., and Kattenhorn, S.A., 2012, A new interpretation of deformation rates in the Snake River Plain and adjacent Basin and Range regions from GPS measurements: *Geophysical Journal International*, v. 189, p. 101–122, doi:10.1111/j.1365-246X.2012.05370.x.
- Peng, X., and Humphreys, E.D., 1998, Crustal velocity structure across the eastern Snake River Plain and the Yellowstone swell: *Journal of Geophysical Research*, v. 103, p. 7171–7186, doi:10.1029/97JB03615.
- Petrik, F.E., 2008, Scarp Analysis of the Centennial Normal Fault, Beaverhead County, Montana and Fremont County, Idaho [M.S. thesis]: Bozeman, Montana, Montana State University, 267 p., 5 plates.
- Pierce, K.L., and Morgan, L.A., 1992, The track of the Yellowstone hotspot: Volcanism, faulting, and uplift, in Link, P.K., Kuntz, M.A., and Platt, L.B., eds., *Regional Geology of Eastern Idaho and Western Wyoming*: Geological Society of America Memoir 179, p. 1–53.
- Pierce, K.L., and Morgan, L.A., 2009, Is the track of the Yellowstone hotspot driven by a deep mantle plume?—Review of volcanism, faulting, and uplift in light of new data: *Journal of Volcanology and Geothermal Research*, v. 188, p. 1–25, doi:10.1016/j.jvolgeores.2009.07.009.
- Press, W.H., Flannery, B.P., Teukolsky, S.A., and Vetterling, W.T., 1989, *Numerical Recipes*: Cambridge, UK, Cambridge University Press, 1256 p.
- Richins, W.D., Pechmann, J.C., Smith, R.B., Langer, C.J., Goter, S.K., Zollweg, J.E., and King, J.J., 1987, The 1983 Borah Peak, Idaho, earthquake and its aftershocks: *Bulletin of the Seismological Society of America*, v. 77, p. 694–723.
- Rodgers, D.W., Hackett, W.R., and Ore, H.T., 1990, Extension of the Yellowstone Plateau, eastern Snake River Plain, and Owyhee Plateau: *Geology*, v. 18, p. 1138–1141, doi:10.1130/0091-7613(1990)018<1138:EOTYPE>2.3.CO;2.
- Rodgers, D.W., Ore, H.T., Bobo, R.T., McQuarrie, N., and Zentner, N., 2002, Extension and subsidence of the eastern Snake River Plain, Idaho, in Bonnicksen, B., White, C.M., and McQuarrie, N., eds., *Tectonic and Magmatic Evolution of the Snake River Plain Volcanic Province*: Idaho Geological Survey Bulletin 30, p. 121–155.
- Sheriff, S.D., and Stickney, M.C., 1984, Crustal structure of southwestern Montana and east-central Idaho—Results of a reversed refraction line: *Geophysical Research Letters*, v. 11, p. 299–302, doi:10.1029/GL011i004p0299.
- Smith, R.B., and Arabasz, W.J., 1991, Seismicity of the Intermountain Seismic Belt, in Slemmons, D.B., Engdahl, E.R., Zoback, M.D., and Blackwell, D.D., eds., *Neotectonics of North America: Boulder, Colorado, Geological Society of America, Decade Map Volume 1*, p. 185–221.
- Smith, R.P., Jackson, S.M., and Hackett, W.R., 1996, Paleoseismology and seismic hazards evaluations in extensional volcanic terrains: *Journal of Geophysical Research*, v. 101, p. 6277–6292, doi:10.1029/95JB01393.
- Sparlin, M.A., Braille, L.W., and Smith, R.B., 1982, Crustal structure of the eastern Snake River Plain determined from ray trace modeling of seismic refraction data: *Journal of Geophysical Research*, v. 87, p. 2619–2633, doi:10.1029/JB087iB04p02619.
- Stachnik, J.C., Dueker, K., Schutt, D.L., and Yuan, J., 2008, Imaging Yellowstone plume-lithosphere interactions from inversion of ballistic and diffusive Rayleigh wave dispersion and crustal thickness data: *Geochemistry Geophysics Geosystems*, v. 9, p. 1–21, doi:10.1029/2008GC001992.
- Stanley, W.D., 1982, Magnetotelluric soundings on the Idaho National Engineering Laboratory Facility, Idaho: *Journal of Geophysical Research*, v. 87, p. 2683–2691, doi:10.1029/JB087iB04p02683.
- Stein, S., and Gordon, R.G., 1984, Statistical tests of additional plate boundaries from plate motion inversions: *Earth and Planetary Science Letters*, v. 69, p. 401–412, doi:10.1016/0012-821X(84)90198-5.
- Stickney, M.C., 1997, Seismic Source Zones in Southwestern Montana: Montana Bureau of Mines and Geology Open-File Report 366, 52 p.
- Stickney, M.C., 2007, Historic earthquakes and seismicity in southwestern Montana: *Northwest Geology*, v. 36, p. 167–186.
- Stickney, M.C., and Bartholomew, M.J., 1987, Seismicity and late Quaternary faulting of the northern Basin and Range Province, Montana and Idaho: *Bulletin of the Seismological Society of America*, v. 77, p. 1602–1625.
- Stoeser, D.B., Green, G.N., Morath, L.C., Heran, W.D., Wilson, A.B., Moore, D.W., and Van Gosen, B.S., 2005, Preliminary Integrated Geologic Map Database for the United States Central States: Montana, Wyoming, Colorado, New Mexico, Kansas, Oklahoma, Texas, Missouri, Arkansas, and Louisiana—The State of Montana: U.S. Geological Survey Open-File Report 2005-1351, scale 1:500,000.
- Stüwe, K., 2002, *Geodynamics of the Lithosphere: An Introduction*: Berlin, Springer-Verlag, 449 p.
- Suppe, J., Powell, C., and Berry, R., 1975, Regional topography, seismicity, Quaternary volcanism, and the present-day tectonics of the western United States: *American Journal of Science*, v. 275-A, p. 397–436.
- U.S. Geological Survey, 2007, Quaternary Fault and Fold Database for the United States: <http://earthquake.usgs.gov/regional/qfaults/> (accessed April 2007).
- Wessel, P., and Smith, W.H.F., 1998, New, improved version of the Generic Mapping Tools released: *Eos (Transactions, American Geophysical Union)*, v. 79, p. 579, doi:10.1029/98EO00426.
- Young, R.A., and Lucas, J.E., 1988, Exploration beneath volcanics: Snake River Plain, Idaho: *Geophysics*, v. 53, p. 444–452, doi:10.1190/1.1442476.
- Yuan, H., Dueker, K., and Stachnik, J., 2010, Crustal structure and thickness along the Yellowstone hotspot track: Evidence for lower crustal outflow from beneath the eastern Snake River Plain: *Geochemistry Geophysics Geosystems*, v. 11, Q03009, doi:10.1029/2009GC002787.
- Zentner, N.C., 1989, Neogene Normal Faults Related to the Structural Origin of the Eastern Snake River Plain, Idaho [M.S. thesis]: Pocatello, Idaho, Idaho State University, 48 p.

MANUSCRIPT RECEIVED 19 JANUARY 2012

REVISED MANUSCRIPT RECEIVED 2 APRIL 2013

MANUSCRIPT ACCEPTED 30 APRIL 2013

Printed in the USA